## General Disclaimer

## One or more of the Following Statements may affect this Document

- This document has been reproduced from the best copy furnished by the organizational source. It is being released in the interest of making available as much information as possible.

- This document may contain data, which exceeds the sheet parameters. It was furnished in this condition by the organizational source and is the best copy available.

- This document may contain tone-on-tone or color graphs, charts and/or pictures, which have been reproduced in black and white.

- This document is paginated as submitted by the original source.

- Portions of this document are not fully legible due to the historical nature of some of the material. However, it is the best reproduction available from the original submission.

Produced by the NASA Center for Aerospace Information (CASI)

(NASA-CR-145865) INTERPRETATION OF SURFACE FEATURES AND SURFACE PROCESSES ON MARS (Virginia Univ.) 39 p HC $4.00 CSCL 08M
N76-13539
Unclas
G3/42 05363

# INTREPRETATION OF SURFACE FEATURES AND SURFACE PROCESSES ON MARS

Technical Report
Contract No. NGR 47-005-172

Submitted to:

NASA Scientific and Technical Information Facility
P. O. Box 8757
Baltimore/Washington International Airport
Maryland 21240

Submitted by:

Mohamed Gad-el-Hak
Assistant Professor
Engineering Science and Systems

Alan Howard
Associate Professor
Environmental Sciences

Jeffery B. Morton
Associate Professor
Engineering Science and Systems

Deborah Pierce
Research Assistant

SCHOOL OF ENGINEERING AND APPLIED SCIENCE

RESEARCH LABORATORIES FOR THE ENGINEERING SCIENCES

UNIVERSITY OF VIRGINIA
CHARLOTTESVILLE, VIRGINIA 22901

DEC 1975
RECEIVED
NASA STI FACILITY
INPUT BRANCH

Report No. ESS-4021-101-75
December 1975

# INTREPRETATION OF SURFACE FEATURES AND SURFACE PROCESSES ON MARS

Technical Report
Contract No. NGR 47-005-172

Submitted to:

NASA Scientific and Technical Information Facility
P. O. Box 8757
Baltimore/Washington International Airport
Maryland 21240

Submitted by:

Mohamed Gad-el-Hak
Assistant Professor
Engineering Science and Systems

Alan Howard
Associate Professor
Environmental Sciences

Jeffery B. Morton
Associate Professor
Engineering Science and Systems

Deborah Pierce
Research Assistant

Department of Engineering Science and Systems
RESEARCH LABORATORIES FOR THE ENGINEERING SCIENCES
SCHOOL OF ENGINEERING AND APPLIED SCIENCE
UNIVERSITY OF VIRGINIA
CHARLOTTESVILLE, VIRGINIA

and

Department of Environmental Sciences
UNIVERSITY OF VIRGINIA
CHARLOTTESVILLE, VIRGINIA

Report No. ESS-4021-101-75

December 1975

Copy No._____

## 1. Introduction

The importance of eolian erosion and deposition on Mars is now unquestioned. The studies undertaken during the past four years under this project have provided some insight into the nature of eolian processes from a viewpoint which has been nearly neglected in the past. We believed that in order to interpret the eolian land forms of Mars, it is necessary to have a sufficient understanding of the physics of eolian transport and deposition on Earth to develop scaling laws which will allow us to scale processes and forms to the vastly different surface and atmospheric regime of Mars. In particular, would the eolian landforms found on Earth be present under the thinner atmosphere and stronger wind regime, and if present, how would the size and shape of these land forms compare with those on Earth?

During the first three years of this research one of us (A.H.) conducted field and aerial photography surveys of some eolian-dominated landforms on earth (in the United States and Peru). During the past year the emphasis has been on wind tunnel studies of the flow field around models of these eolian forms to attempt to reproduce a more extensive map of the flow. This effort has given us information useful in elucidating the mechanics determining the form and scale of eolian bedforms and the interactions between topography and regional winds which result in sand deposits. The shift in research emphasis reflects the need for quantitative verification and extension of hypotheses generated during the field studies.

## 2. Areas of Activities

The wind tunnel studies have been directed primarily in the following five areas:

I – Simulation of the atmospheric boundary layer in a wind tunnel,

II – Velocity profile measurements around different models in the desert boundary layer; estimating shear stress distributions on the model surfaces,

III – Developing appropriate flow visulization techniques for better understanding of the flow around the different models,

IV – Streamline mapping using tuft photographs,

V – Roughness contrast experiments.

## 3. Simulation of Atmospheric Boundary Layer in a Wind Tunnel

Techniques have been developed for simulating the lower 100 meters or so of a neutral atmosphere. The initial effort was directed at adapting these techniques to flow over a desert. This involved simulating an appropriate velocity profile and ground roughness.

In the wind tunnel used, the incoming air is initially forced through a contraction (C.F. figure 1), producing a more uniform velocity profile with turbulence levels at approximately 0.1%. It then passes through two grids (#1 and #2) designed to produce high turbulence levels similar in magnitude to those observed in the atmosphere. A final grid of variable-spaced bars (#3) produces the desired logarithmic velocity profile, corresponding to the desired $z_o$ [1]. The models are embedded into the roughened floor.

For a neutrally stable atmosphere, the mean velocity profile near the ground (the first 100 meters or so, where Coriolis effects are negligible) can be written as:

$$U(z) = \frac{u_*}{K} \ln \frac{z}{z_o}$$

where $u_*$ is the friction velocity ($= \sqrt{\frac{\tau_o}{\rho}}$, $\tau_o$ is the shear stress at the surface and $\rho$ is the air density), k is the von Karman constant ($\simeq 0.4$), and $z_o$ is the roughness height [2].

A convenient scale factor for our facilities has been found to be 315:1. Thus, different dunes have been scaled down by that factor; an atmospheric boundary layer of height 190 m. is roughly represented by our tunnel height, 60 cm., and a natural roughness of 7.2 cm. is simulated in our tunnel by $z_o \simeq 0.023$ cm. Figure 2 is a semi-logarithmic plot of the mean

velocity profiles at different distances (x) downstream from the logarithmic rod grid (rod diameter, d, is 1.9 cm.). The profiles follow the given logarithmic velocity profile formula. Figure 3 shows the turbulence level profiles. This simulation of the atmospheric boundary layer is quite satisfactory and compares well with naturally grown boundary layers in wind tunnels [1, 3, 4, 5].

## 4. Velocity Profile Measurements Around Different Models in the Desert Boundary Layer

Velocity profile measurements were made around four different topographic forms in the simulated desert flow field of the wind tunnel. The first three models are scale models of barchan dunes that exist in an area near the Salton Sea, California; the fourth model is a conical "hill" with a slope of 33 degrees. Detailed mean velocity profiles at different locations on the cone and on one of the barchan dunes were measured. Figure 4 shows the locations at which profiles were measured on the dune, called barchan #1 for convenience, a contour map of barchan #1 is shown in figure 5. Profiles were taken at the intersections of lines A, A' (the dune's crest), B, and C with lines 1 through 13; additional profiles were measured at various locations in front of and behind the dune. A less extensive set profiles was measured around the two other barchan dune models.

The profiles were measured at a constant reference tunnel speed 10 m/s; the effect of changing the reference speed, $\bar{U}_R$, was studied, and it will be shown later that speed changes in the range 5-10 m/s have no effect on the non-dimensionalized profiles. Only the component of the mean velocity profile parallel to the flow direction in the wind tunnel was measured, although lateral velocities could be estimated from the longitudinal component and the streamline maps resulting from flow visualization measurements.

The models were inserted at a distance 287 cm downstream from the rod grid. Reference tunnel speed was monitored by a Mariam manometer model 34FBZ connected to two static pressure holes in the tunnel walls. Mean velocity profiles and turbulence intensities were measured using

two types of hotwire probes, a Disa type 55F11, 5 micron, platinum-plated, tungsten, straightwire, with a sensitive length of 1.25 mm, and a Disa type 55P12 45° probe, which facilitates measurements close to the windward surfaces of the topographic forms. A Disa type 55D01 constant temperature anemometer was used in conjunction with a Disa type 55D01 linearizer and a Disa type 55D29 auxiliary unit. An overheat ratio of 0.6 and a linearizer exponent setting of 2.2 were normally used, producing an output linearly proportional to the velocity fluctuations within a set frequency range from D.C.to 5 KHz.

Figure 6 shows a composite diagram of selected velocity profiles taken around barchan #1. Figure 7 shows a composite of velocity profiles around the cone. In each diagram, an undisturbed velocity profile, U, measured 10 cm upwind of the models, is included for comparison. The The composite profiles include only a few of the profiles measured and were selected because of the significant flow trends they show. The profiles not shown in the composite diagrams are being subjected to different types of analysis, to be described later.

From a study of figure 6, it is possible to deduce a few flow characteristics along line 7. (Refer to figure 4). Velocity increases as the flow travels up the windward face of the dune toward the crest. All of the profiles rejoin the undisturbed logarithmic velocity profiles at a height of approximately 12 cm above the ground; thus the dune significantly affects the flow up to a height 6 times its own height. A "kink" in all of the curves occurs at a height 10 cm above the ground. The kink was a repeatable phenomenon and unexpected; we are unable to explain its appearance or significance at the present time. In the lee of the dune, measurements are difficult due to the inability of a hot wire to follow reverse flows [17]. However, the reverse flow region extends

only to about 2 cm above the ground, and from the profiles one could estimate the location of the "dead zone" behind the dune. Similar observations can be made about the flow around the cone [6, 7] (figure 7). Additional composite diagrams have been carefully studied for flow trends.

Additional experiments were performed in studying the flow around Barchan #1. As mentioned previously, the tunnel reference speed was changed to investigate any possible effects on the velocity profiles. Profiles at several points were measured for tunnel speeds, $\bar{U}_R$, of 5, 6, 7, 8 and 10 m/s. It was found that if the velocity profiles were nondimensionalized using the appropriate reference speed, the profiles would collapse with a percentage error of about 4%, on the average. Figure 8 shows sample velocity profiles taken (at point 7A) at reference speeds of 5 and 10 m/s; the two profiles were nondimensionalized by dividing the velocities by the appropriate reference speed. It can be seen that the profiles closely coincide.

Another experiment was performed to determine the necessity of using the simulated boundary layer for measuring barchan profiles. The grids and roughness element were removed from the tunnel, and profiles were taken at several points on the dune. Figure 9 shows a typical comparison between the free-stream profile at point 7A and the logarithmic profile at the same location. It is clear from the graph that the curves are entirely dissimilar. Therefore, it was established that the simulated environment was necessary if meaningful velocity profiles around the barchan dune were to be produced.

A third experiment was conducted to investigate the effects of change of wind direction on the profiles. The dune was rotated through several known angles, producing the effect of a change in wind direction, and, at a reference tunnel speed of 10 m/s, velocity profiles were taken at several

points for each angle. Analysis of the results of this experiment is still not completed, although a sheltering effect has been noted at certain points when successive angles of rotation move the point more in the lee of the dune's bulk. Figures 10 and 11 show the sheltering effect described; at position 13A' (on the crest of the dune), as the dune is rotated from $30^{\circ}$ to $-30^{\circ}$ the velocities close to the surface decrease as the point 13A' is moved to the lee of the main part of the dune, sheltering the point from the wind. At 2A'(2 crest) a similar effect is evident as the dune is rotated; in this case the velocities decrease as the dune is rotated from $-30^{\circ}$ to $20^{\circ}$ because 2A'is on the opposite wing of the dune. As z increases, the angular effect ceases, as the profiles join the undisturbed logarithmic profile.

## 5. Developing Appropriate Flow Visualization Techniques for Better Understanding of the Flow Around the Different Models

Hotwire measurements made around the models provide accurate information about the relative speeds of the flow at different points in space. The ability of the hotwire to indicate direction of flow is limited and involves a tedious process. The hotwire has an angular cosine sensitivity to the flow and it may be rotated to find the direction of flow. However, it must be maneuvered back to the position of interest after it is rotated through the desired angle, and the prongs on which the wire is mounted can cause some interference with the actual flow if they are blocking the sensitive part of the wire.

An alternate method of determining flow direction is flow visualization. There are many methods of flow visualization used for determining streamlines around models; three principal methods were investigated for this project. The first, and most successful, method used was tufting. Thin strips of tissue paper were mounted at various points on and around the dune, carefully glued in place to have no directional bias initially. Under wind action, the tufts aligned themselves in the direction of the wind. Photographs were taken at different exposures to determine "instantaneous" wind direction as well as "average" wind direction, and the latter were used in the construction of streamline maps. A sample streamline map is included in the next section. Figure 12 (a) shows a sample tuft photograph taken at 1/2 second exposure; 12 (b) was taken at an exposure time of 2 seconds.

The second method of flow visualization employed was smoke injection. A smoke generator, the schematic design of which is reproduced in figure 13, produced a jet of smoke, initially laminar, which was illuminated on one

plane by a laser light. The resulting flow could be seen in that plane clearly with the eye and somewhat less clearly in the photographs. A Tri-x film was used and developed with UGF high-speed developer to yield an effective ASA number of 3200. The chief drawback of the smoke flow visualization was that, although the flow could be seen clearly when the only velocity was that of the smoke emerging from the orifice, once the tunnel wind was turned on, the smoke dispersed so rapidly that it became too thin to scatter enough light for an effective photograph. Other drawbacks were poor photograph quality and the limitation imposed on the planes of illuminated flow due to the inaccessibility of lower planes.

The third method of flow visualization used was the oil drop method. Colored drops of oil were quickly placed on the dune's surface through a hypodermic syringe and the wind was turned on. The resulting tracks left by the colored oil as it travelled over the dune's surface were to have been the streamlines. The oil drop method was successful when a high speed jet of air was aimed at the model. For speeds attainable in the wind tunnel (5 - 10 m/s), however, gravitational effects outweighed wind effects on the oil drops.

Thus, tuft flow visualization was ultimately the most successful streamline indicator employed of the three flow visualization methods.

## 6. Streamline Mapping Using Tuft Photographs Estimate for Shear Stress Distributions on the Surface

Estimates of erosion and deposition rates of sand on the surface of a barchan dune are of primary importance in any analysis to explain the self-preserving nature of the dune's shape. Both streamline mapping and detailed mapping of the wind velocities close to the dune's surface are crucial factors in determining erosion and deposition rates. Using the tufting method of flow visualization mentioned in section 5 and the near surface velocity profiles described in section 4, it is possible to construct streamline maps for the barchan dune models.

Figure 14 is a map of the near surface streamlines for barchan #1 when the tunnel reference speed is 10 m/s. Streamlines on the upwind surface of the dune are the result of analysis of tuft photographs. Several photographs are used to construct one map; average tuft direction is determined for each tuft from the photographs, and the resulting direction vectors are plotted on a diagram of the dune. The vectors are extrapolated and joined to form streamlines. Allen [8] used flow visualization methods in a water flume to find streamlines for a dune similar to the barchan represented in figure 14. Allen's streamlines (dashed lines) for the wind flow in the lee of the dune are added to figure 14 to give a complete picture of the flow around the dune.

Quantitative data of the near surface velocity profiles obtained (section 4) by the hotwire probe provides a good indication of direction of wind flow over a barchan dune. Streamline mapping using near velocities is still in progress. Measurements as close as 2.5 mm to the dune's surface have been made at approximately 50 different points on the model. Sand transport occurs chiefly through the mechanism of saltation [9, 10, 11,

12, 13, 14], a process which ejects the grains into a trajectory to an average height above the dune's surface. Thus, the near surface velocities on the dune are influential in determining the path of the sand grains. Detailed calculations relating the near surface velocities and slope angles of the dune to the resulting grain paths and, thus, to the total movement of sand around the barchan dune, are in progress. Further experimentation with tufting to determine streamlines will be carried out to aid in the quantitative analysis of the flow.

The use of shear stress probes, Disa-type 55R47, has been investigated for determining the shear stress at the surface of the dune. Shear stress measurements will be compared to near surface velocity measurements to determine a possible correlation between them. The principle source of error in the use of the shear stress probe has been found to be in its calibration process. A sample calibration curve is given in figure 15. The probe is calibrated to give a value of shear stress vs. voltage output in the following manner: the probe is mounted on a flat surface, perpendicular to the oncoming wind; a pitot tube is located close to the probe and is moved vertically. For each of several tunnel speeds, a velocity profile is measured with the pitot tube. The output voltage from the shear stress probe is linearized and is constant for a constant reference tunnel speed. From the velocity profiles, values of the friction velocity, $u_*$, and hence the shear stress $\tau_o$ at the surface, are obtained for each reference tunnel speed. Values of $\tau_o$ are plotted against the corresponding values of voltage obtained from the shear stress probe. The scatter of the points on the calibration curve is a result of the uncertainty inherent in determining $u_*$ from the velocity profiles.

## 7. Roughness Contrast Experiments

When wind conditions responsible for preserving isolated barchan dunes change, a different sand form results. According to Bagnold [9], strong winds emerging from a direction other than that of the prevailing gentle wind may be the cause of a transition from barchan dune formations to longitudinal, or seif, dunes, which form long chains parallel to the wind direction. A series of wind tunnel experiments were conducted to determine the flow pattern around longitudinal sand forms, which were represented in the tunnel by 6 m long strips of roughness elements with different $z_o$ values. Similar experiments had been conducted in the field of agriculture to determine the effects of contrast of roughness on soil erosion by wind; soil erosion resulting when the contrast occurred perpendicular to the wind direction was compared to the erosion when the contrast was parallel to the prevailing wind [15, 16].

Several combinations of roughness elements were studied in the wind tunnel, using flow visualization techniques and pitot tube measurements. Stones with an average diameter of 1.4 cm were aligned in 20 cm wide strips on either side of a "smooth" element. The smooth strip varied from cardboard to small pebbles (average d = 0.45 cm). Velocity profiles were measured at several locations along a line perpendicular to the wind direction.

An alternate experiment consisted of replacing the smooth middle layer with the 1.4 cm diameter stones, "sandwiched" between two smooth cardboard strips. Profiles were measured with the stones aligned both parallel and at a slight angle to the wind direction. Figure 16 illustrates two contrast arrangements which were of particular interest. Figure 16 (a) shows the smooth-rough-smooth combination, and 16 (b) shows the alternate rough-smooth-rough arrangement. In both cases, the "smooth" element was cardboard; the

"rough" element consisted of the 1.4 cm diameter stones. Velocity profiles were measured at 5 different locations on a line perpendicular to the wind direction.

Figures 17 and 18 are graphs of the profiles measured in case (a) above. A trend is evident in the graphs; at $z \leq 8$ cm, the flow is at its highest speed at position 5 and progressively decreases in speed as it approaches position 1, at the center of the stones. This trend indicates a crossflow of wind from positions 1 to 5, which is strongest near the floor and weakens with increasing z. At $z \geq 8$ cm, the profiles converge and then reverse slightly (at $z = 16$ cm), indicating a weak crossflow from positions 5 to 1.

Figures 19 and 20 are graphs of the profiles measured in case (b), which also show a crossflow at $z \leq 8$ cm away from the stones and toward the smooth area. The same weak crossflow as for case (a) occurs towards the stones at $z = 17$ cm. In cases (a) and (b), the semilog graphs clearly show the change in effective $z_o$ as the position change.

Tuft photographs taken correlate well with the profile measurements, indicating a deflection away from the stones (and, thus, a crossflow away from them) at low z values, and a slight deflection toward the stones at higher elevations.

## 8. Concluding Remarks

The desired desert boundary layer, with a $z_o$ value of 0.23 mm, was simulated in the wind tunnel and compares satisfactorally with naturally grown boundary layers.

Velocity profiles around four models were measured and significant flow trends were observed. Experiments were conducted to determine the effects of change of wind speed and direction on the flow.

Three flow visualization methods were investigated; the "tufting" method proved to be the most effective in indicating flow trends.

Streamline mapping of the barchan dune is in progress, using flow visualization methods and the results of near velocity profiles. Calculations of sand flow around the barchan are in progress, using the results of streamline mapping and estimates for the shear stress.

Experiments performed on elements of contrasting roughness show consistent crossflow patterns.

## REFERENCES


1. Kokus, M. T., "A Physical Model of the Earth's Atmospheric Surface Layer", M. Sc. Thesis, University of Virginia, 1975.

2. Tennekes, H. and J. L. Lumley, A First Course in Turbulence, MIT Press, 1972.

3. Sundaram, T. R., G. K. Ludwig and F. T. Skinner, "Modeling of the Turbulence Structure of the Atmospheric Surface Layer", AIAA Journal, Vol. 5, 1967.

4. Panofsky, H. A. and J. L. Lumley, The Structure of Atmospheric Turbulence, Interscience, 1964.

5. Cermak, J. E. and S. P. S. Arya, "Problems of Atmospheric Shear Flows and their Simulation", Boundary Layer Meterology, Vol. 1, 1970.

6. Pierce, D. B., "Velocity Profiles around a Cone in a Simulated Atmospheric Boundary Layer", Research Paper, University of Virginia, 1975.

7. Sato, H., Y. Onda and T. Siato, "Laboratory Simulation of Atmospheric Turbulence-Generation of Arbitrary Velocity Distributions and Model Experiment on Flow Around Mt. Fuji", Symposium on Turbulent Diffusion in Environmental Pollution, University of Virginia, 1973.

8. Allen, J. R. L., Current Ripples, North-Holland, 1968.

9. Bagnold, R. A., The Physics of Blown Sand and Desert Dunes, Methuen, 1941.

10. White, B. R., J. D. Iversen, R. Greeley and J. B. Pollack, "Particle Motion in Atmospheric Boundary Layers of Mars and Earth", NASA, TM X-62, 463, 1975.

11. Bagnold, R. A., "The Movement of a Cohesionless Granular Bed by Fluid Flow over it", British Journal of Applied Physics, Vol. 2, 1951.

12. Ford, E. F., "The Transport of Sand by Wind", Transactions of the American Geophysical Union, Vol. 38, 1957.

13. Horikawa, K. and H. W. Shen, "Sand Movement by Wind Action", Beach Erosion Board Corps of Engineers, TM 119, 1960.

14. Belly, P. Y., "Sand Movement by Wind", U. S. Army Corps of Engineers, TM 1, 1964.

15. Chepil, W. S. and N. P. Woodruff, "The Physics of Wind Erosion and its Control", Advances in Agronomy, Vol. 15, 1949.

16. Malina, F. J., "Recent Developments in the Dynamics of Wind Erosion", Transactions of the American Geophysical Union, Vol. 22, 1941.

17. Bradshaw, P., An Introduction to Turbulence and its Measurement, Pergamon Press, 1971

## Figure Captions

Figure 1: Schematic of the wind tunnel test section

Figure 2: Undisturbed velocity profiles at various downstream locations

Figure 3: Turbulence level at various downstream locations

Figure 4: Schematic grid of profile locations (barchan #1)

Figure 5: Contour map of barchan #1

Figure 6: Velocity profiles along line 7 for barchan #1

Figure 7: Velocity profiles around cone

Figure 8: Scaled velocity profiles at 5 and 10 m/s

Figure 9: Comparison between free-stream and logarithmic velocity profiles

Figure 10: Velocity profiles at 13 crest ($13A^1$) with change of wind angle

Figure 11: Velocity profiles at 2 crest ($2A^1$) with change of wind angle

Figure 12: Tuft flow visualization photographs of barchan #1

Figure 13: Schematic of smoke generator

Figure 14: Streamline map of barchan #1

Figure 15: Shear stress probe calibration curve

Figure 16: Roughness contrast experiment

Figure 17: Velocity profiles, inner roughness aisle

Figure 18: Velocity profiles, inner roughness aisle (semi-log plot)

Figure 19: Velocity profiles, outer roughness aisles

Figure 20: Velocity profiles, outer roughness aisles (semi-log plot)

PRECEDING PAGE BLANK NOT FILMED

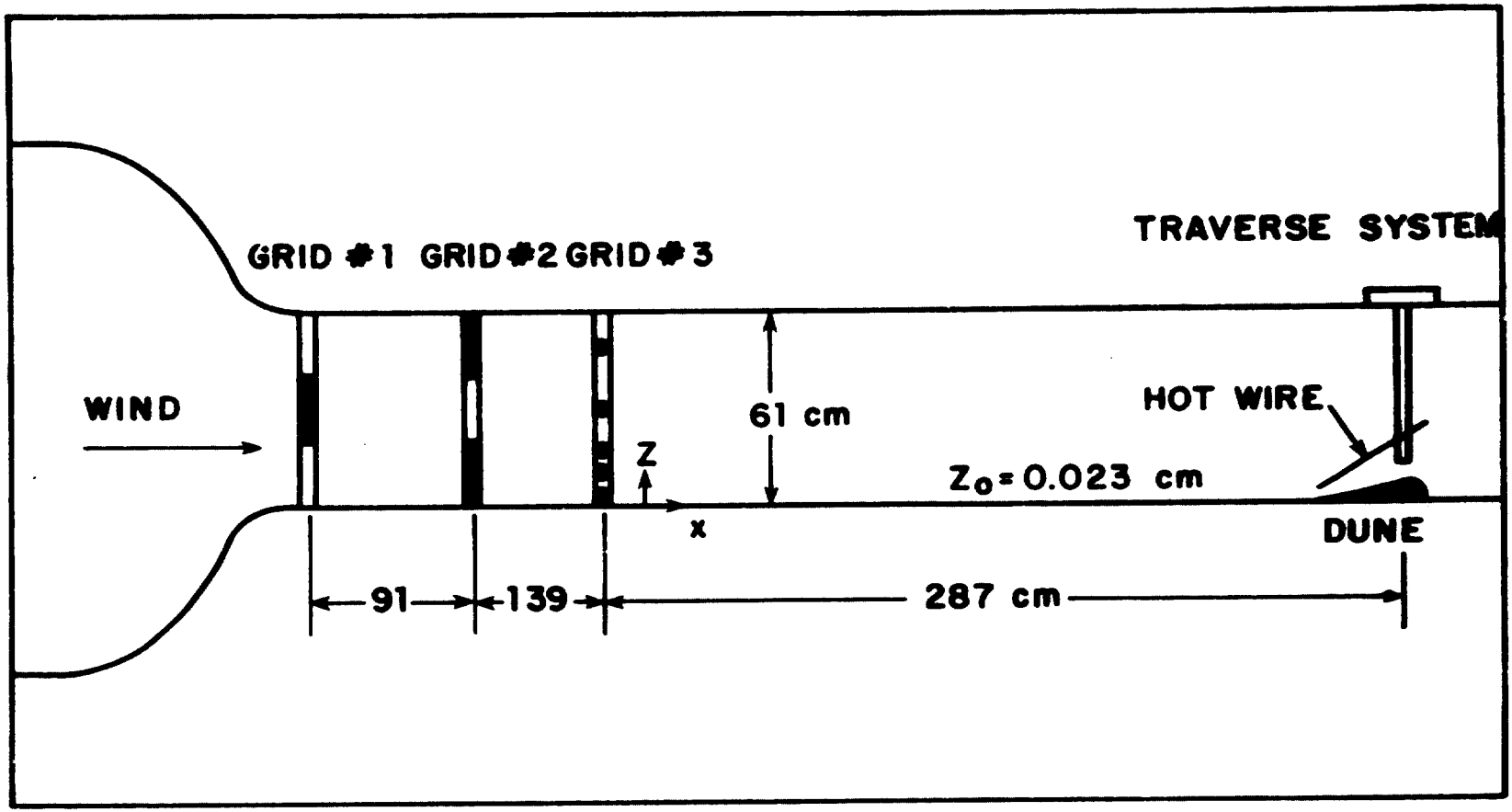


Figure 1: Schematic of the Wind Tunnel Test Section

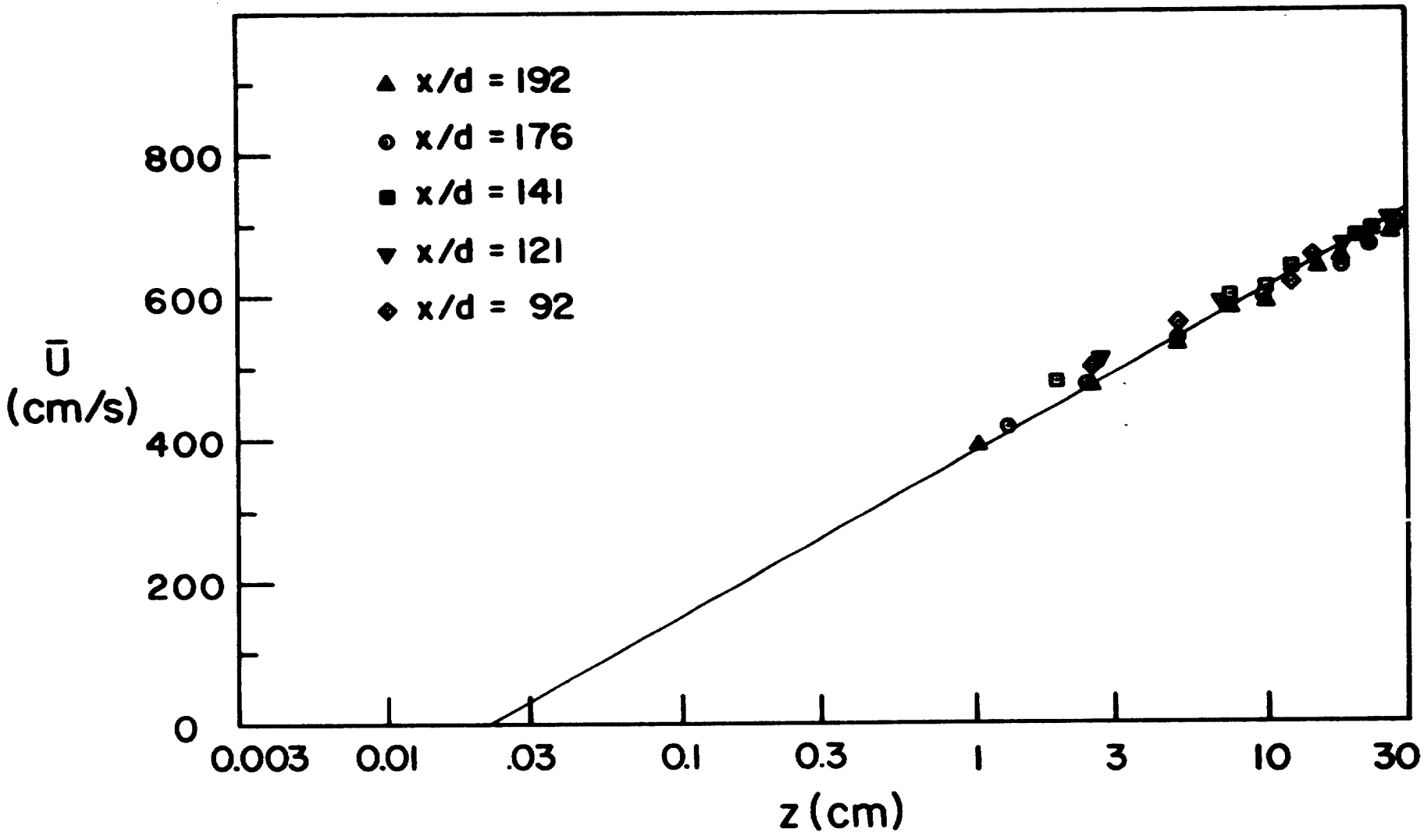


Figure 2: Undisturbed Velocity Profiles at Various Downstream Locations

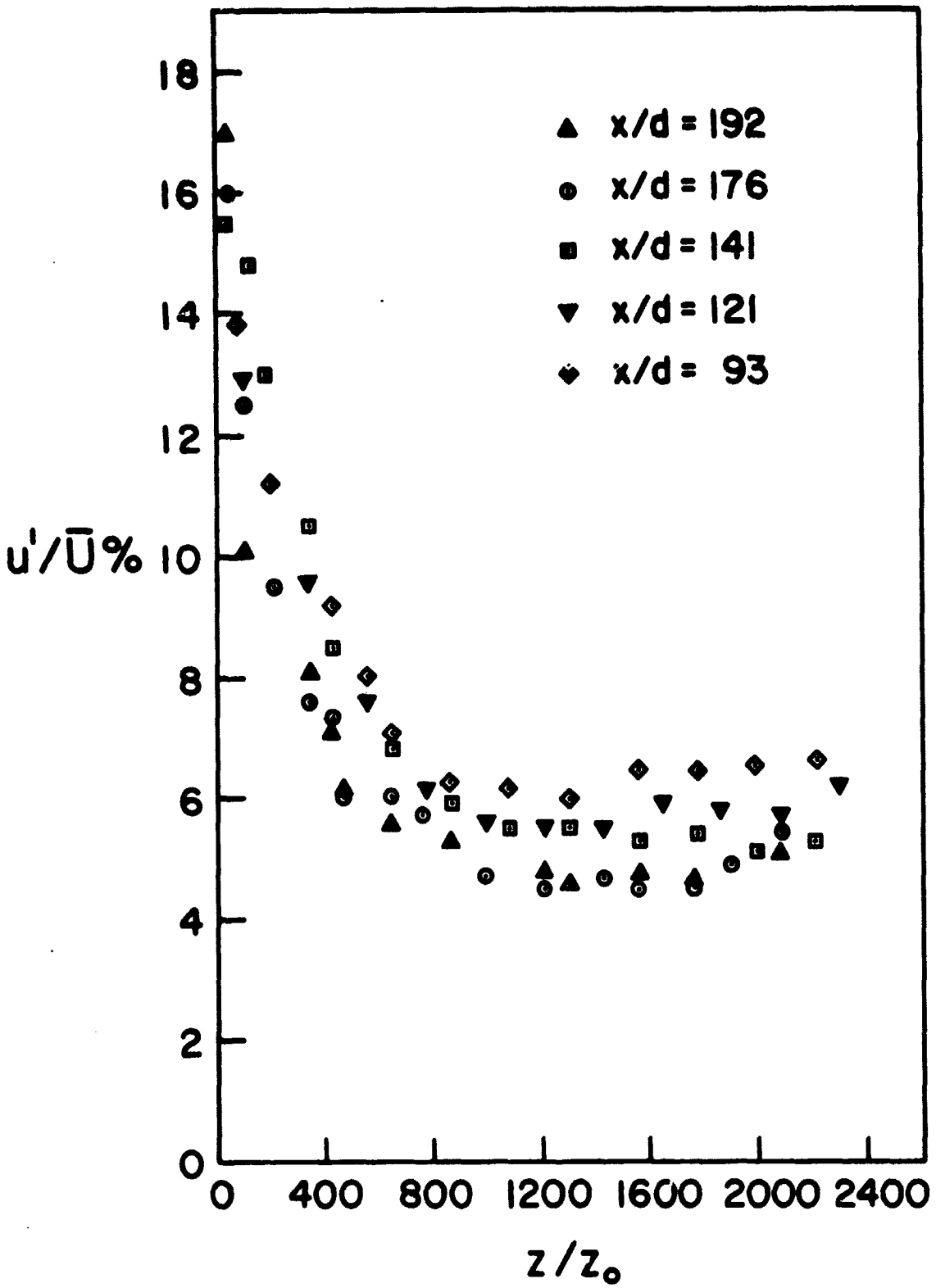


Figure 3: Turbulence Level at Various Downstream Locations

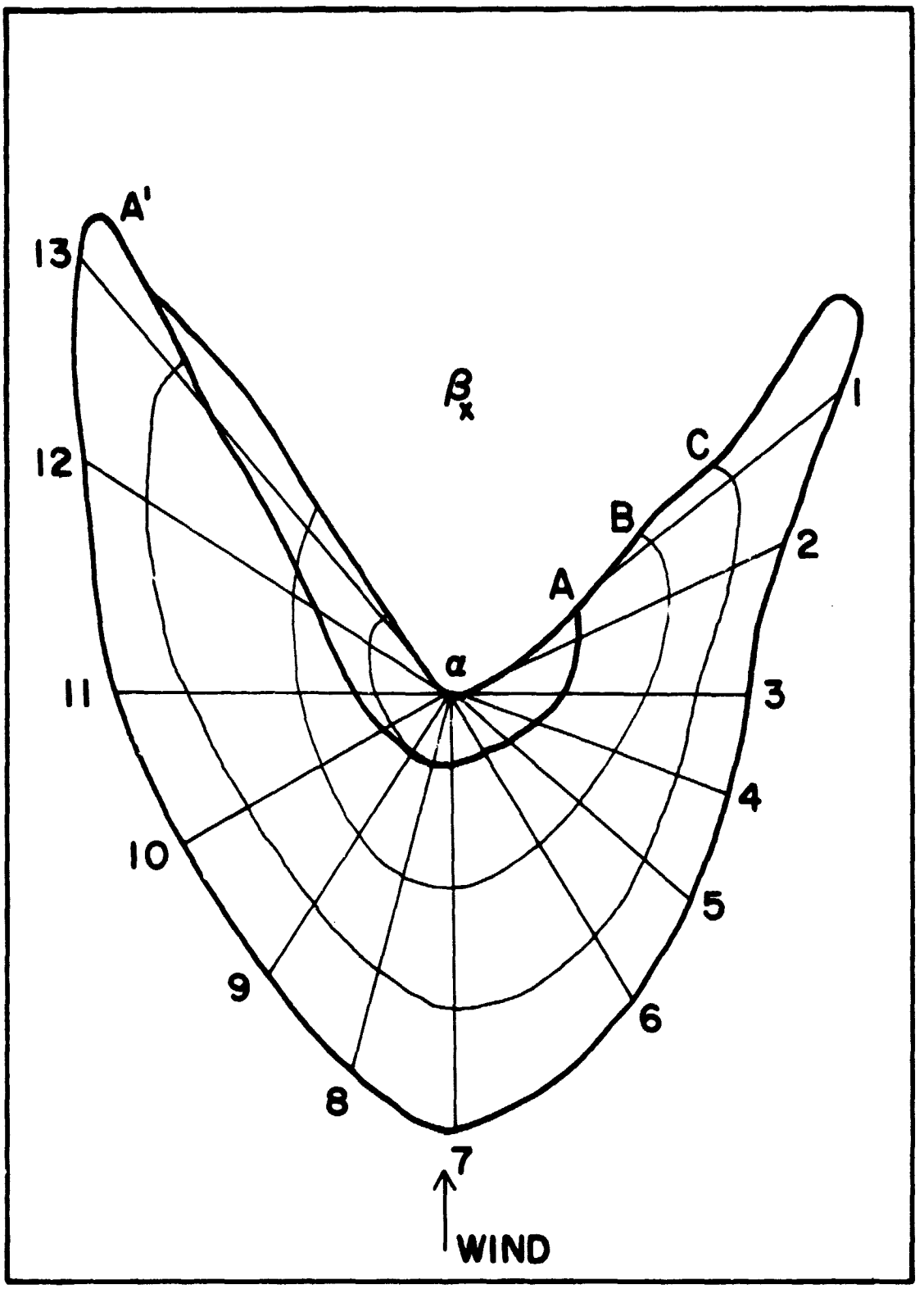


Figure 4: Schematic Grid of Profile Locations (Barchan #1)

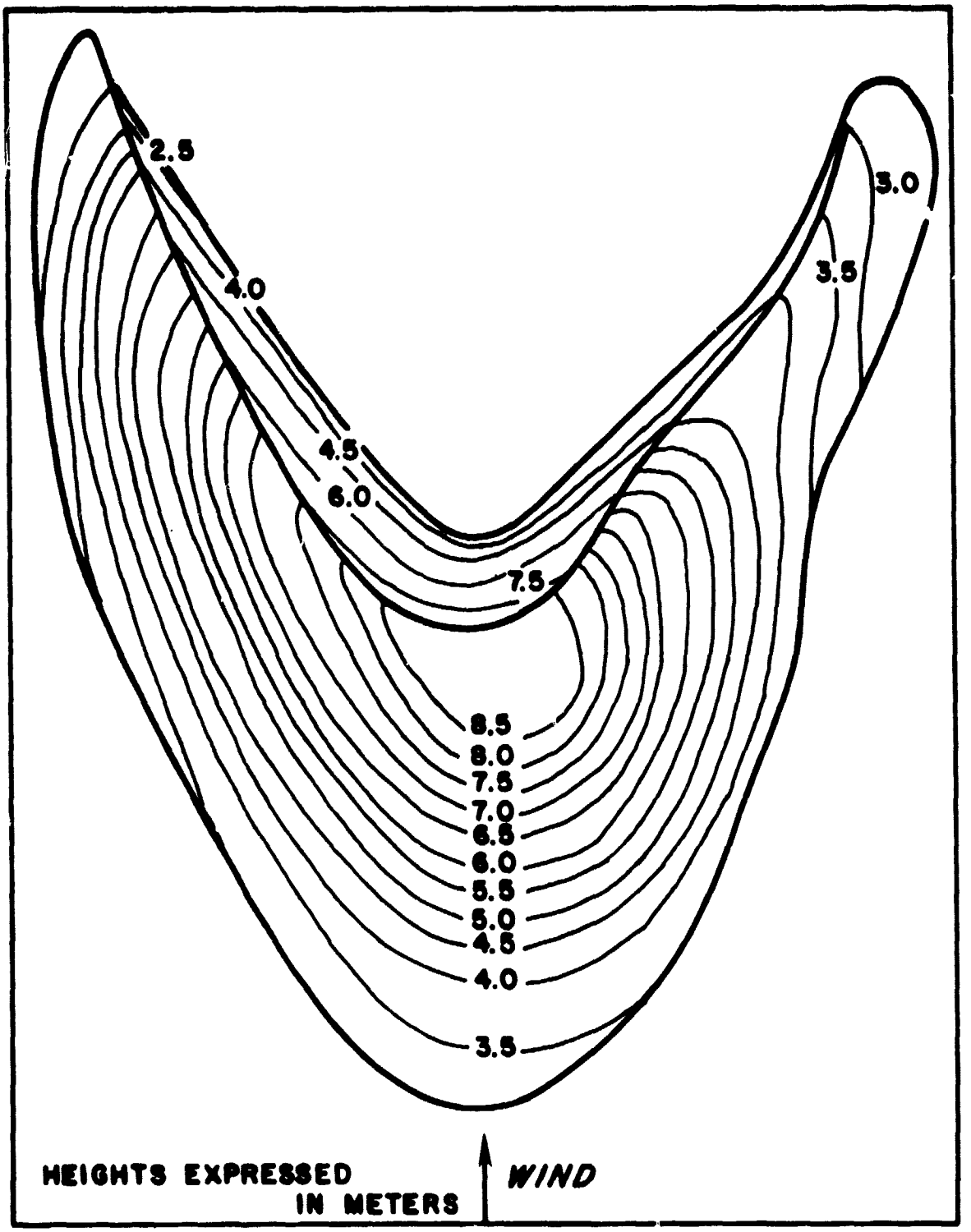


Figure 5: Contour Map of Barchan #1

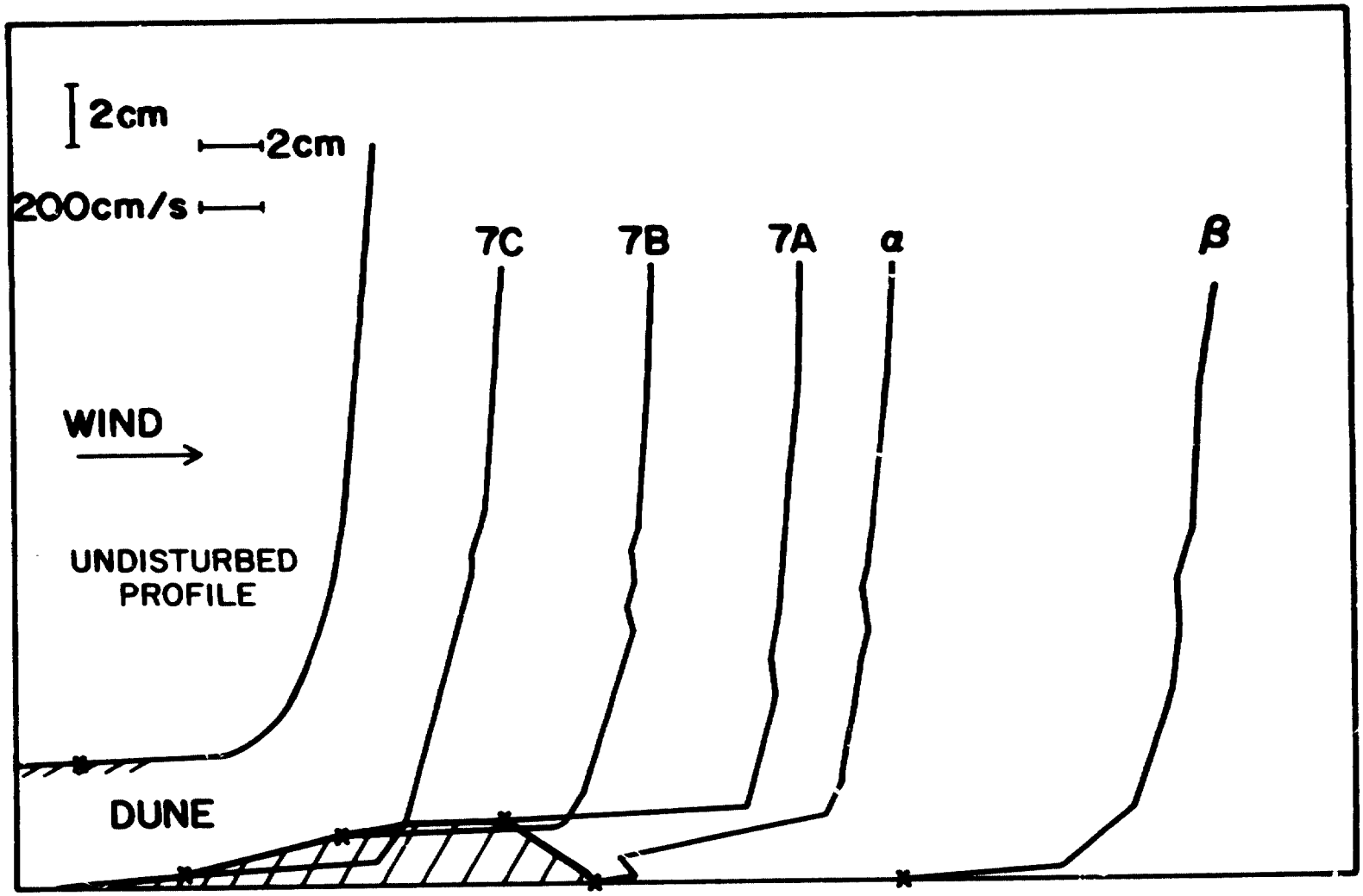


Figure 6: Velocity Profiles along Line 7 for Barchan #1

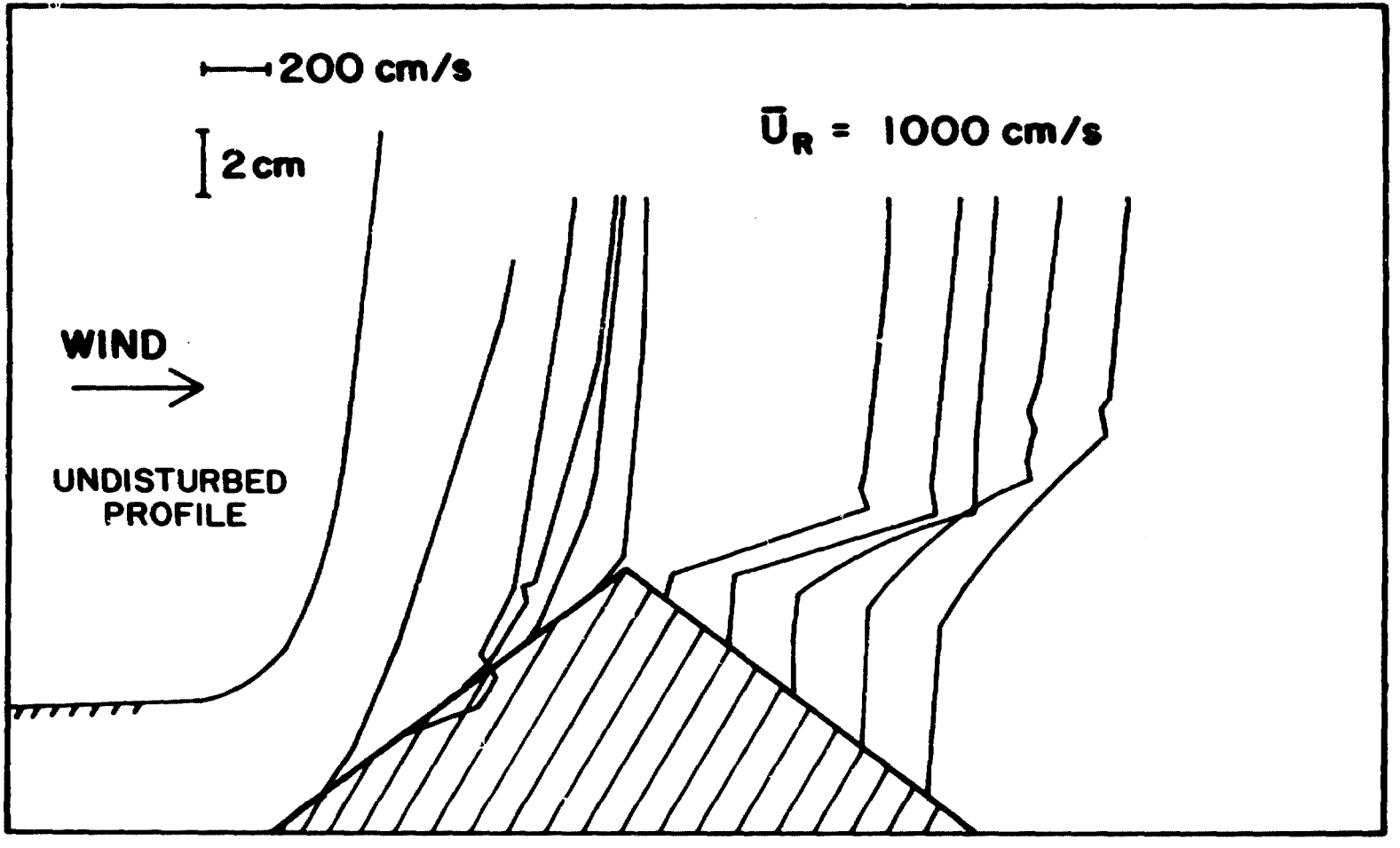


Figure 7: Velocity Profiles around Cone

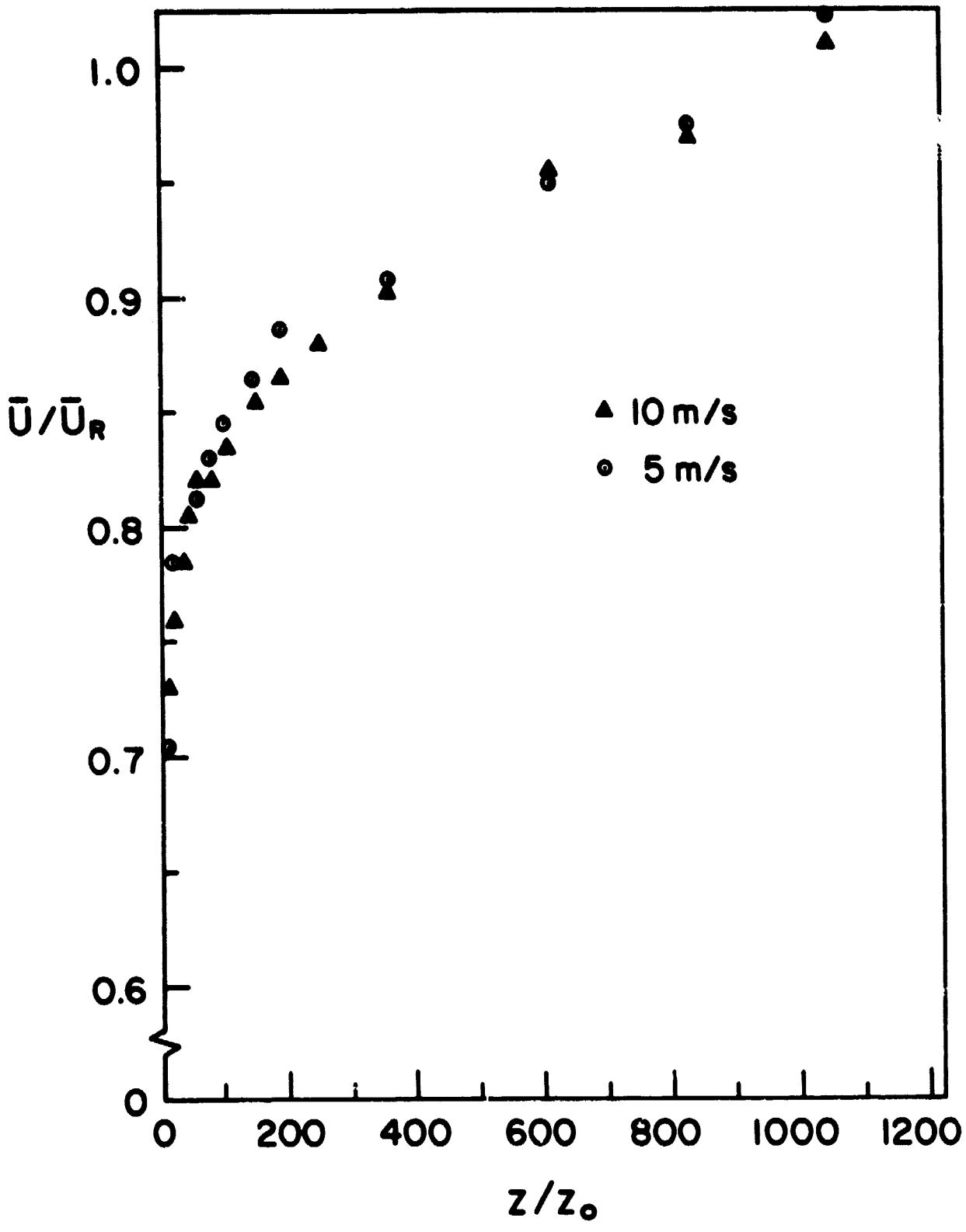


Figure 8: Scaled Velocity Profiles at 5 and 10 m/s

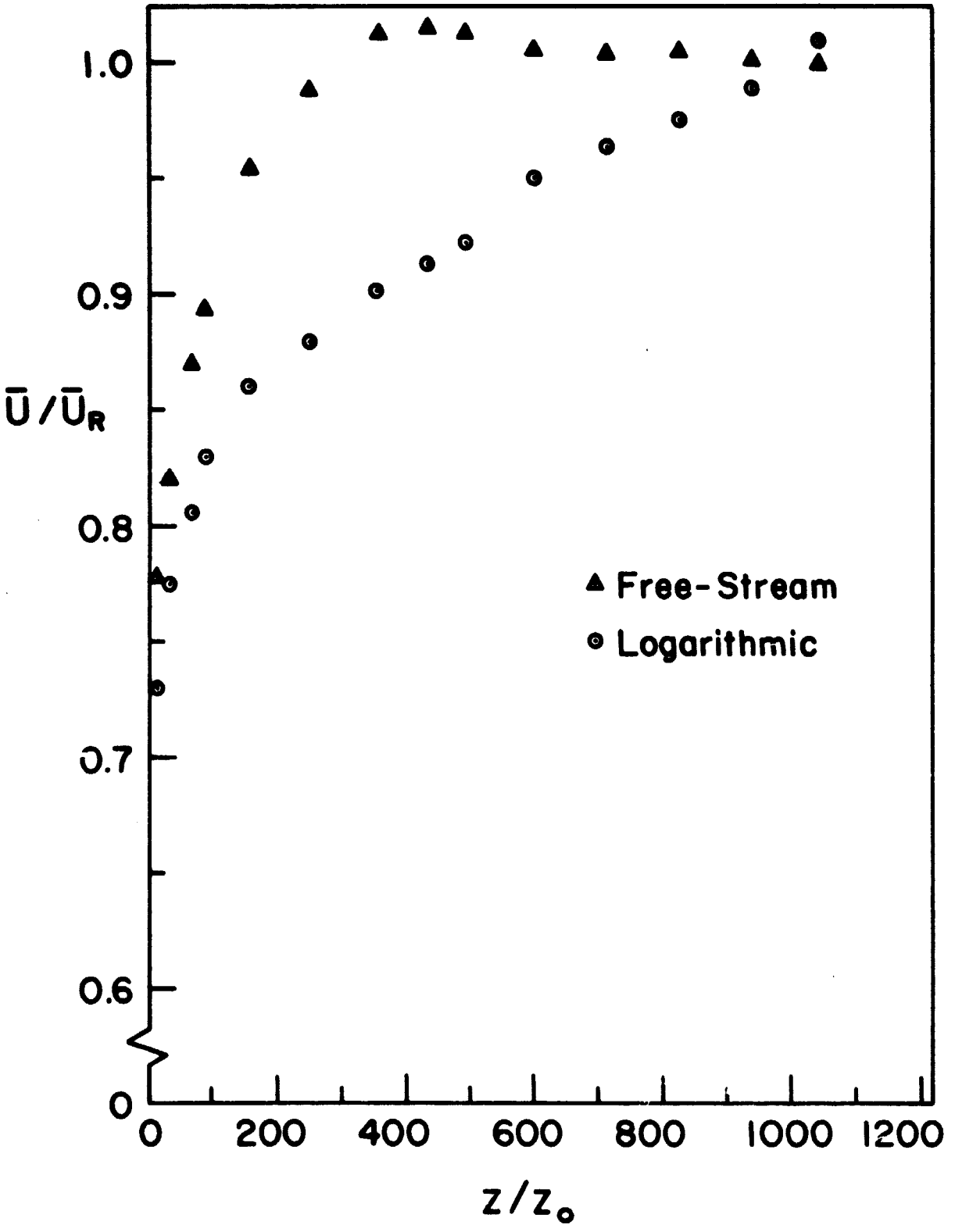


Figure 9: Comparison between Free-Stream and Logarithmic Velocity Profiles

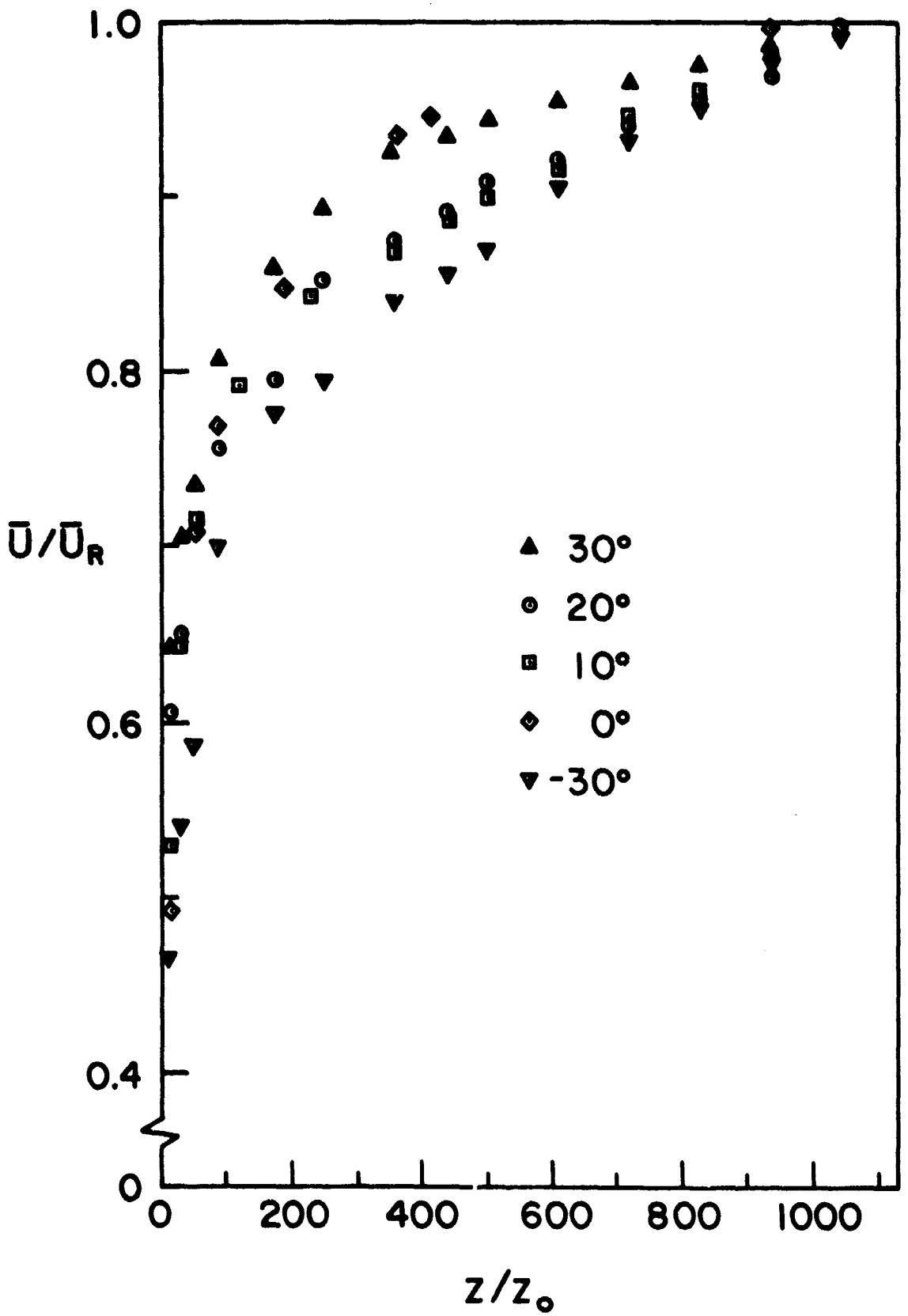


Figure 10: Velocity Profiles at 13 crest (13A') with

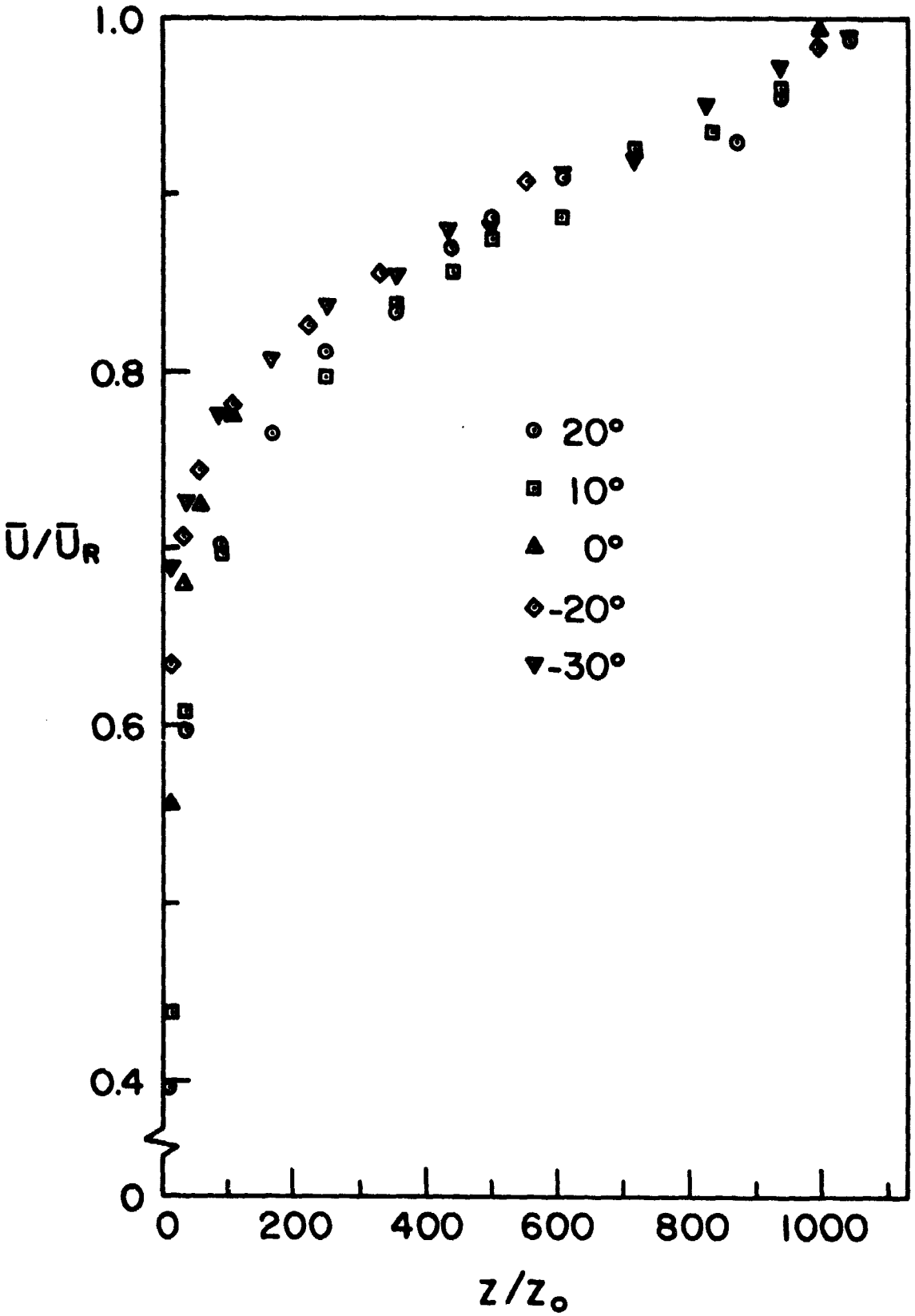


Figure 11: Velocity Profiles at 2 crest (2A') with Change of Wind Angle

Figure 12: Tuft Flow Visualization Photographs of Barchan #1.

ORIGINAL PAGE IS
OF POOR QUALITY

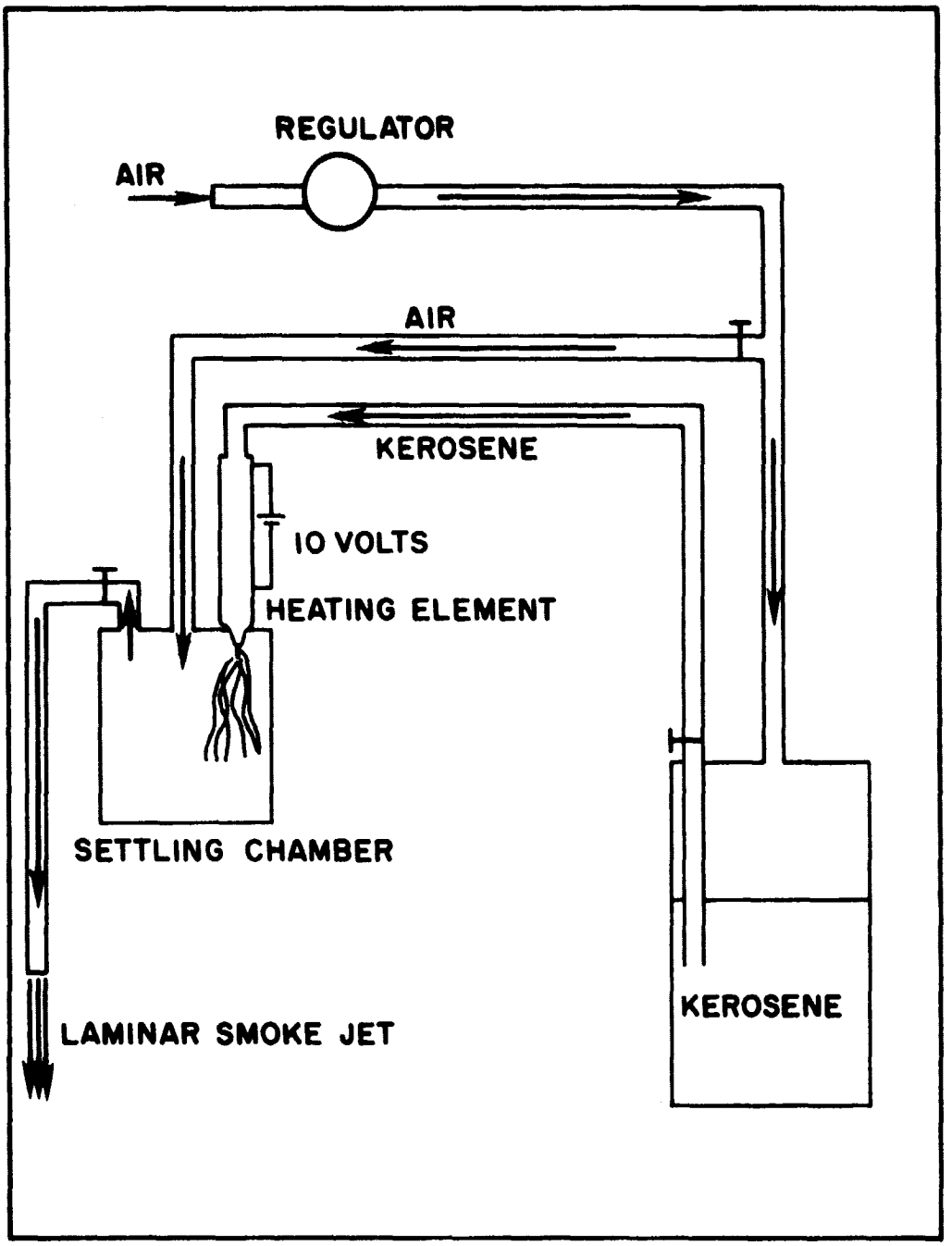


Figure 13. Schematic of Smoke Generator

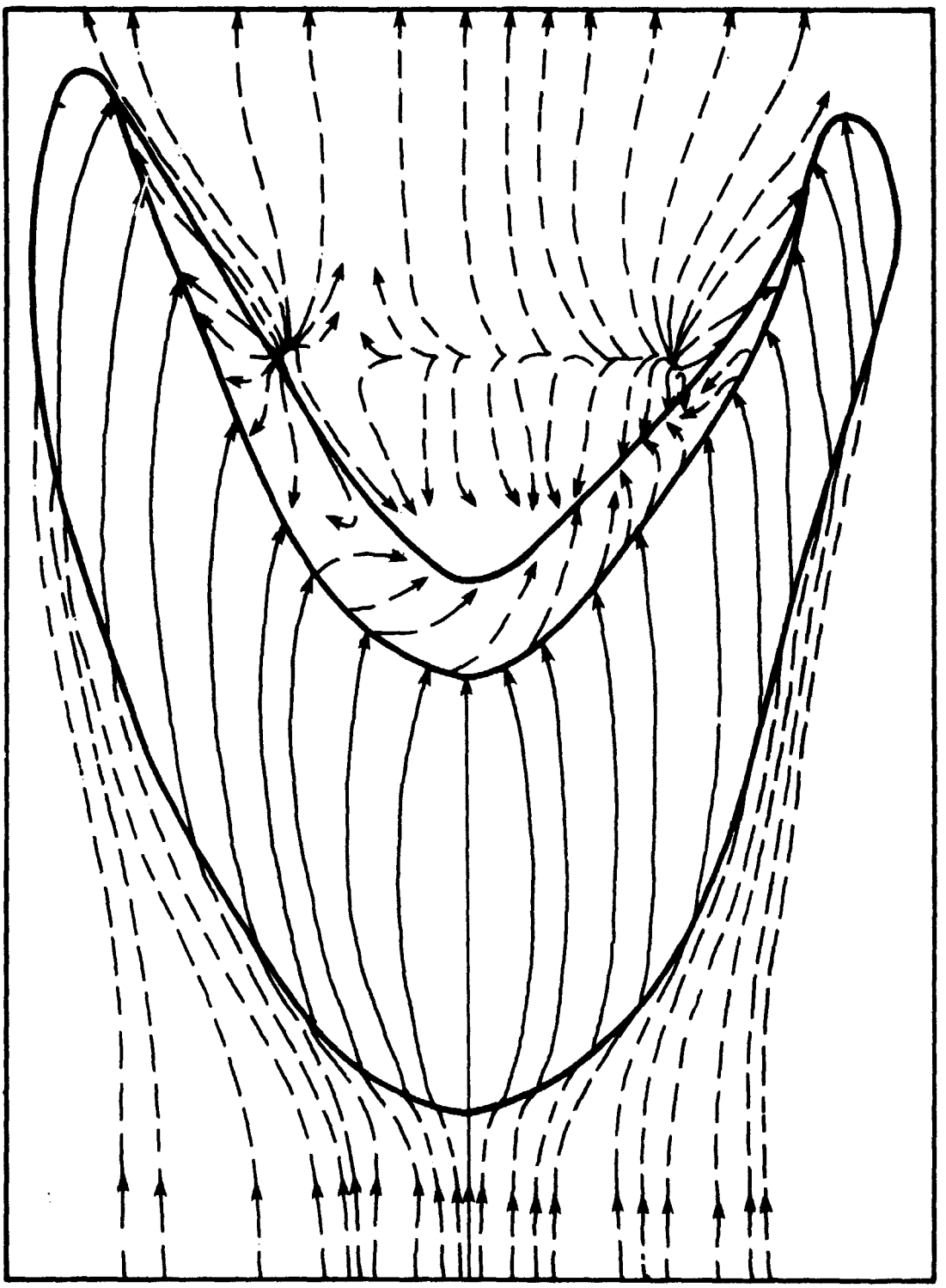

Figure 14: Streamline Map of Barchan #1

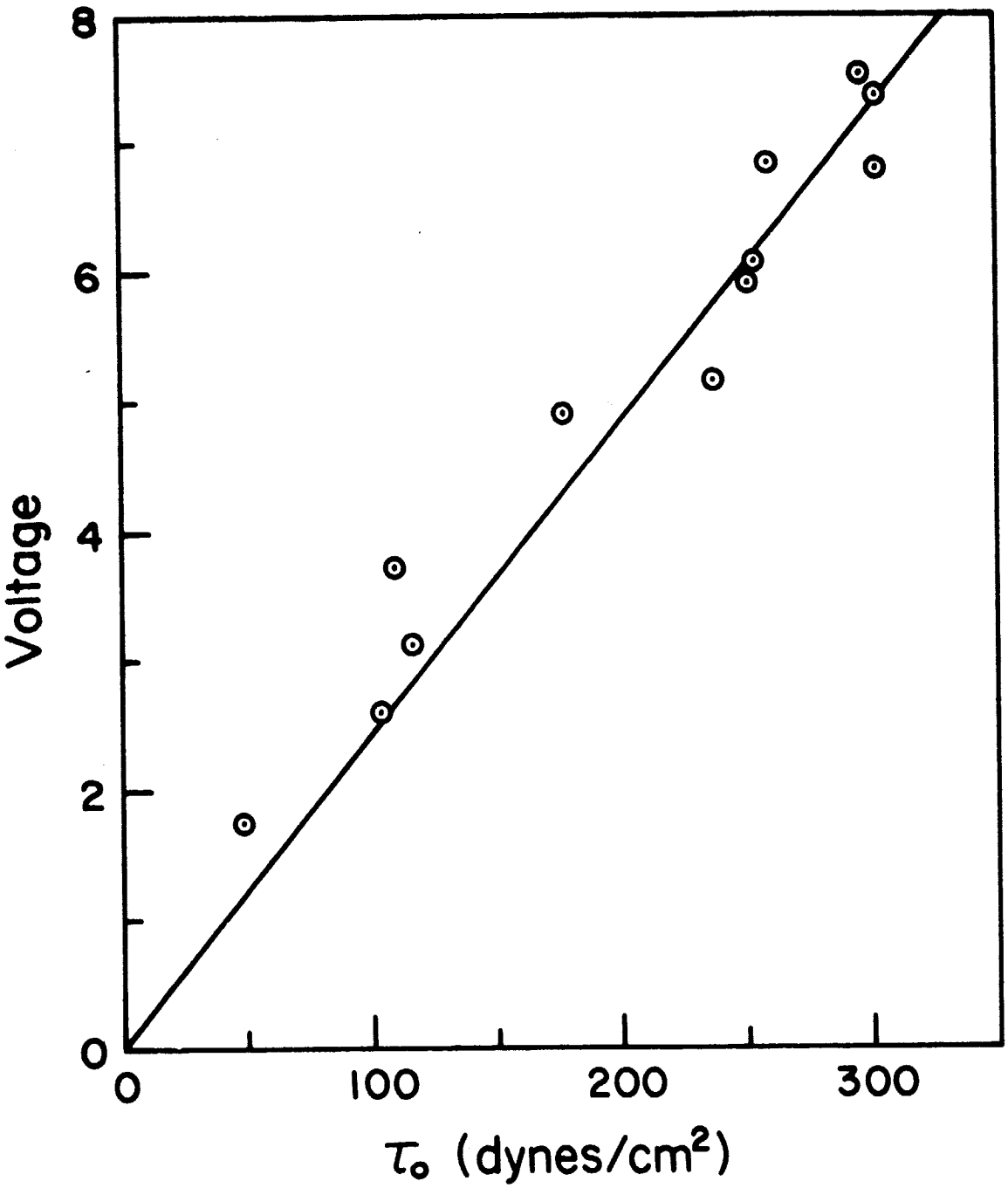


Figure 15: Shear Stress Probe Calibration Curve

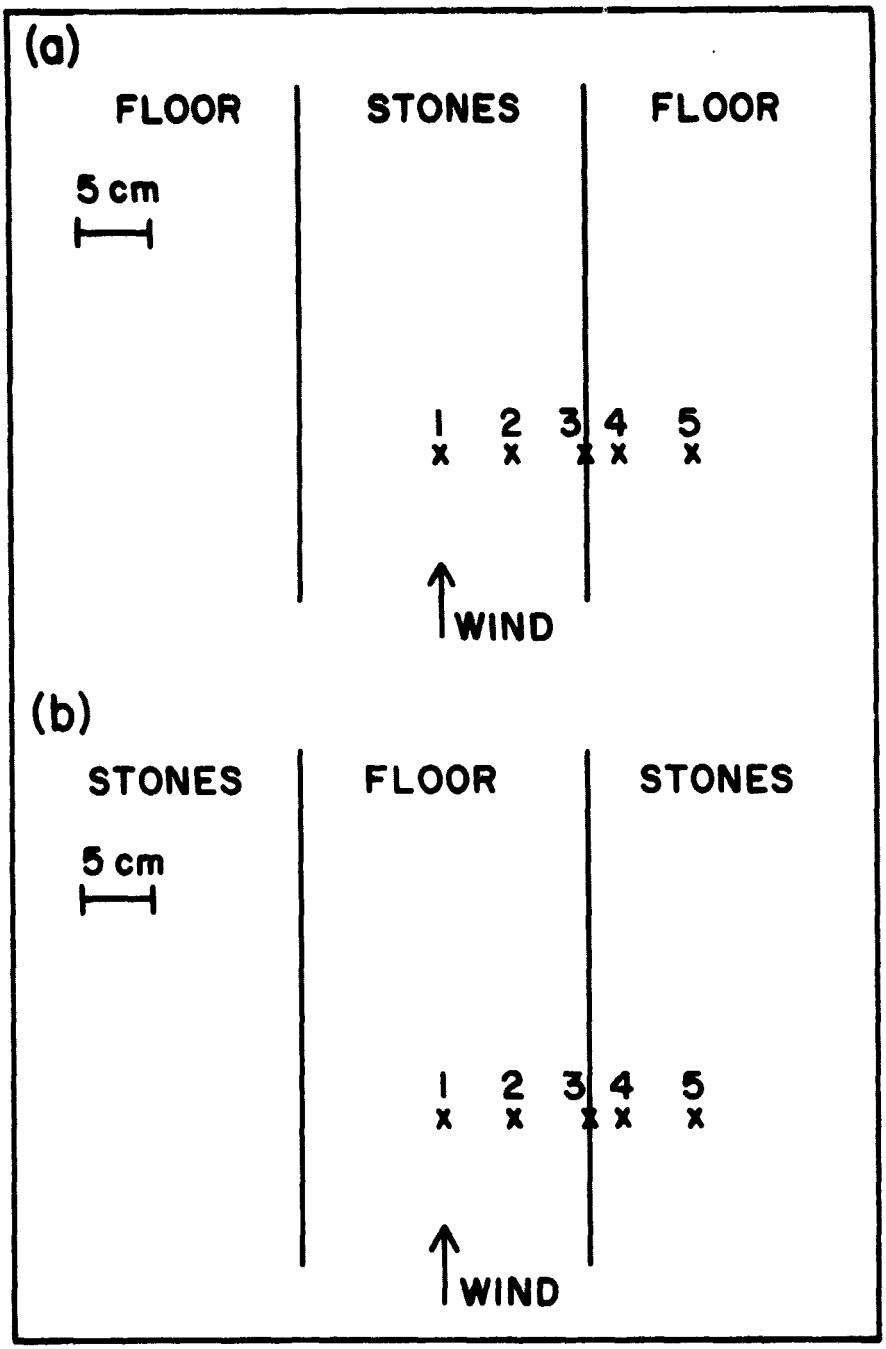


Figure 16: Roughness Contrast Experiment

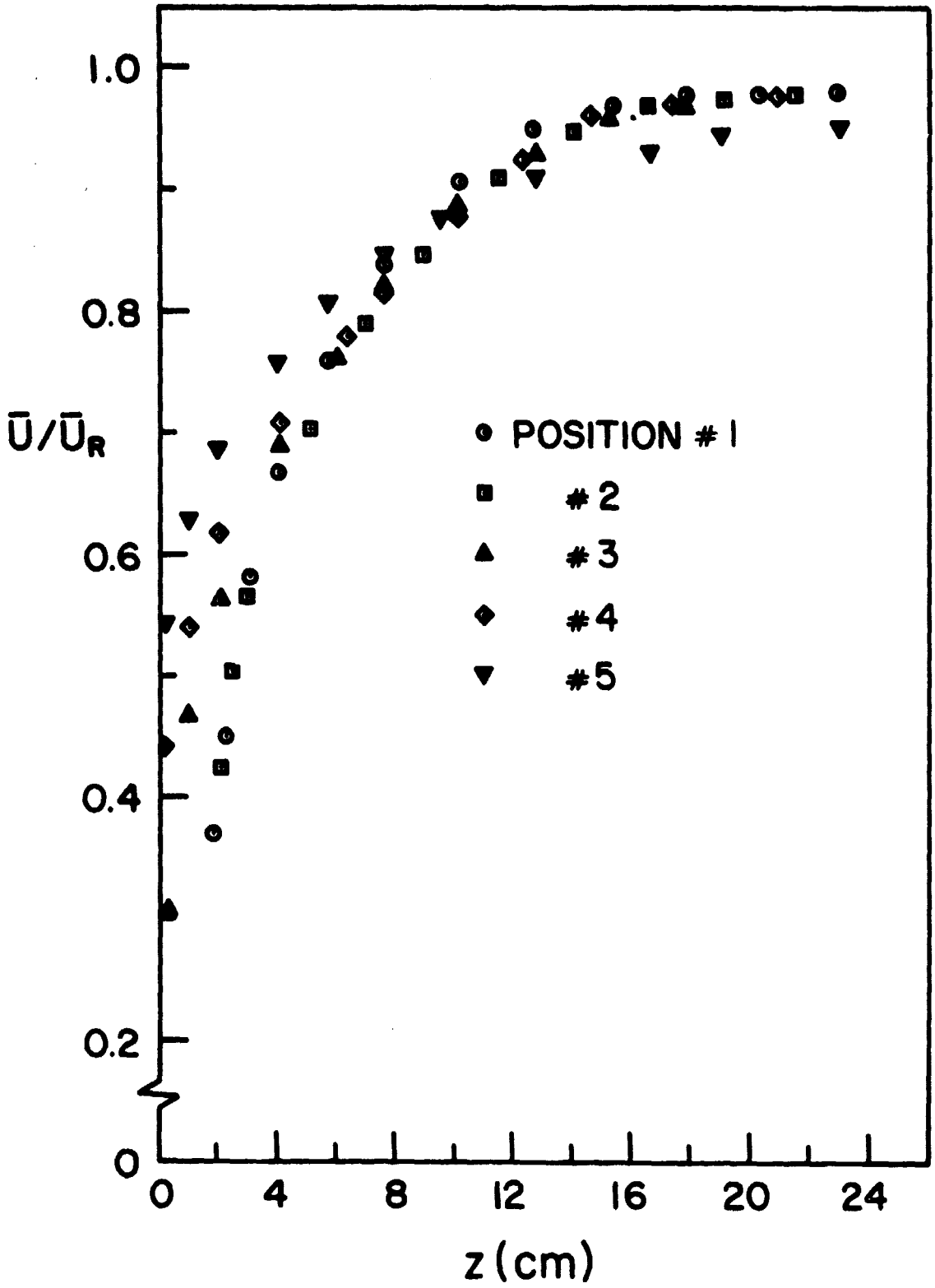


Figure 17: Velocity Profiles, Inner Roughness Aisle

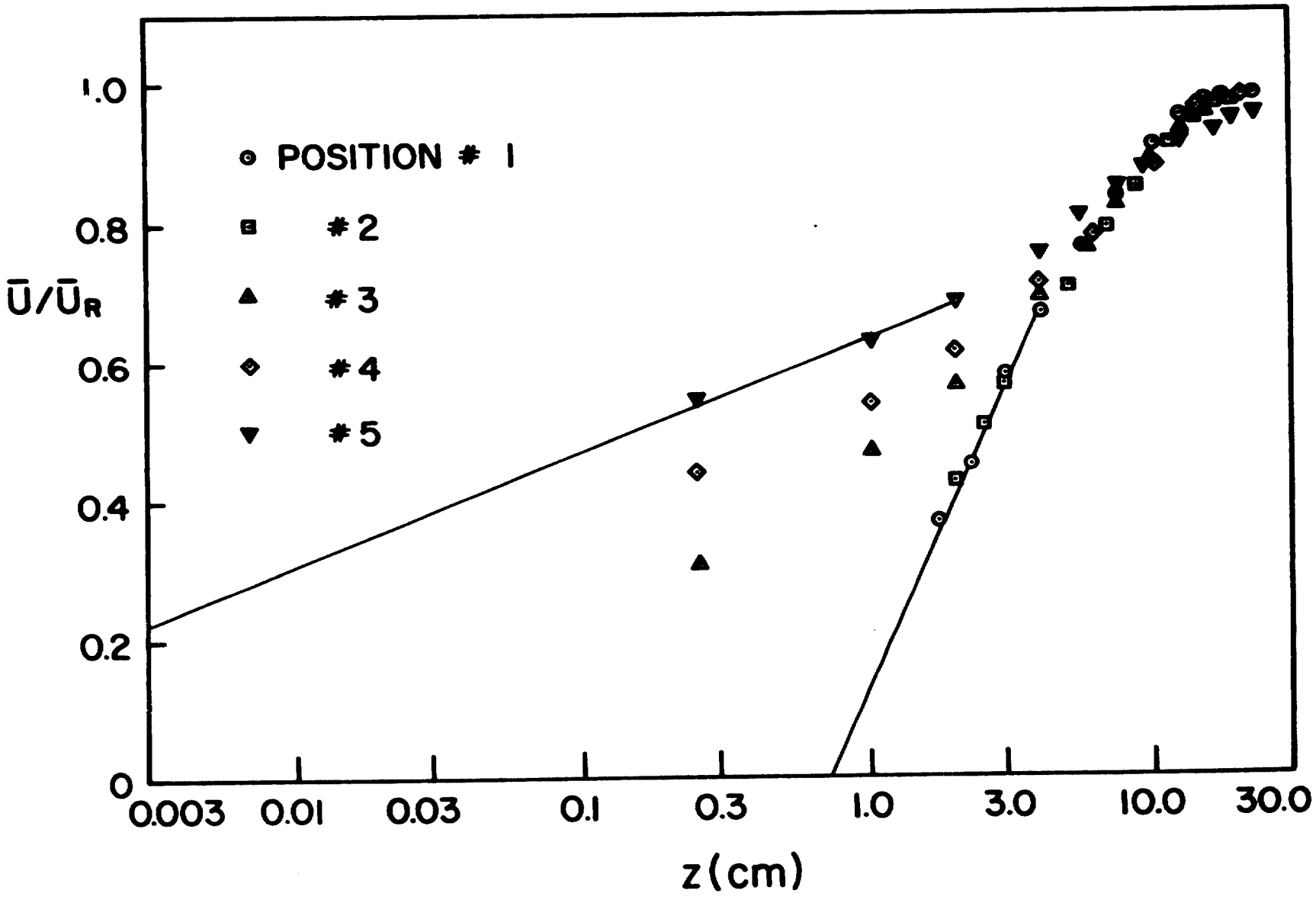


Figure 18: Velocity Profiles, Inner Roughness Aisle

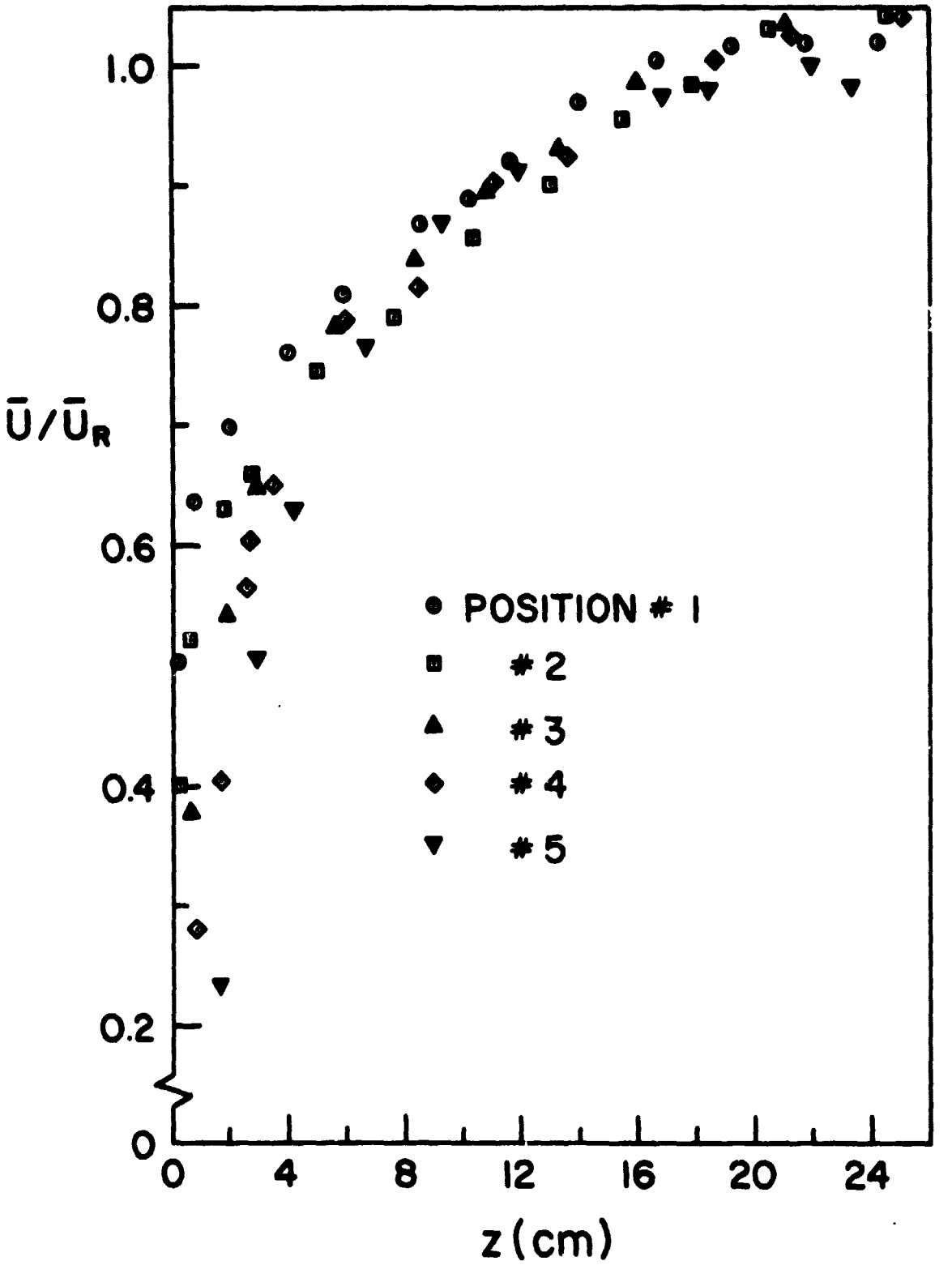


Figure 19: Velocity Profiles, Outer Roughness Aisles

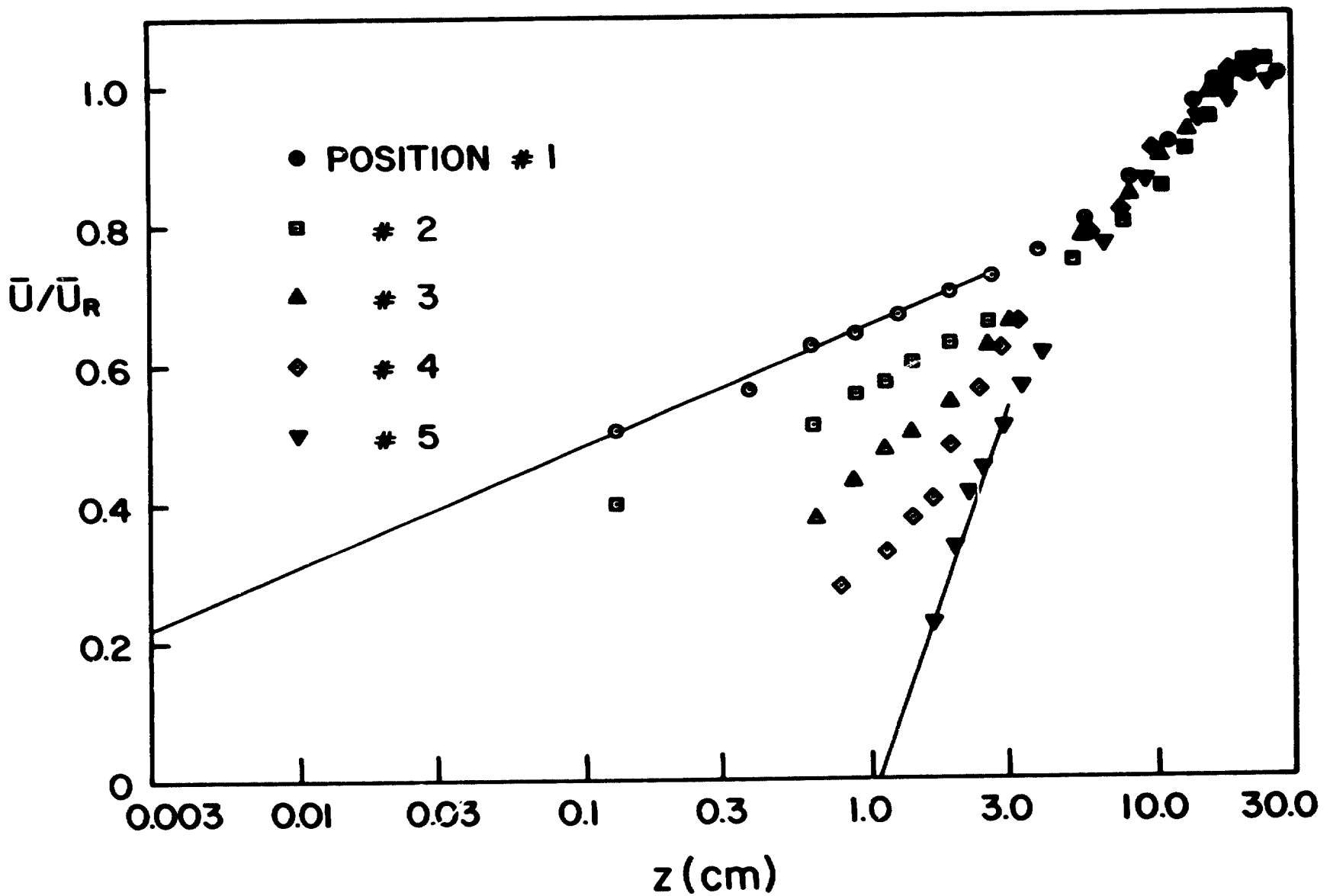


Figure 20: Velocity Profiles, Outer Roughness Aisles